JOURNAL OF MAGNETIC RESONANCE **89,** 496–514 (1990)

Three-Dimensional Triple-Resonance NMR Spectroscopy of Isotopically Enriched Proteins

LEWIS E. KAY, MITSUHIKO IKURA, ROLF TSCHUDIN, AND AD BAX

Laboratory of Chemical Physics, NIDDK, National Institutes of Health, Bethesda, Maryland 20892

Received February 22, 1990

Four new and complementary three-dimensional triple-resonance experiments are described for obtaining complete backbone ^{1}H, ^{13}C, and ^{15}N resonance assignments of proteins uniformly enriched with ^{13}C and ^{15}N. The new methods all rely on ^{1}H detection and use multiple magnetization transfers through well-resolved one-bond J couplings. Therefore, the 3D experiments are sensitive and permit relatively rapid recording of 3D spectra (1–2 days) for protein concentrations on the order of 1 mM. One experiment (HNCO) correlates the amide ^{1}H and ^{15}N shifts with the ^{13}C shift of the carbonyl resonance of the preceding amino acid. A second experiment (HNCA) correlates the intraresidue amide ^{1}H and ^{15}N shifts with the Cα chemical shift. This experiment often also provides a weak correlation between the amide NH and ^{15}N resonances of one amino acid and the Cα resonance of the preceding amino acid. A third experiment (HCACO) correlates the Hα and Cα shifts with the intraresidue carbonyl shift. Finally, a 3D relay experiment, HCA(CO)N, correlates Hα and Cα resonances of one residue with the ^{15}N frequency of the succeeding residue. The principles of these experiments are described in terms of the operator formalism. To optimize spectral resolution, special attention is paid to removal of undesired J splittings in the 3D spectra. Technical details regarding the implementation of these triple-resonance experiments on a commercial spectrometer are also provided. The experiments are demonstrated for the protein calmodulin (16.7 kDa).

Complete assignment of the backbone proton resonances of a protein forms the basis for further detailed conformational studies. For smaller proteins, such assignments can often be obtained from a systematic analysis of COSY, NOESY, and HOHAHA/TOCSY (*1, 2*). For larger proteins, a variety of selective labeling procedures can provide dramatic spectral simplification and thus assist in the assignment process (*3–10*). However, this latter approach is quite labor-intensive since it requires multiple samples with different amino acids labeled in each protein preparation. Recently proposed heteronuclear 3D NMR experiments of uniformly ^{15}N-labeled proteins provide simplification by spreading the crowded NOESY or HOHAHA spectra into a third dimension, the ^{15}N chemical shift (*11–14*). These 3D experiments require only a single sample of uniformly ^{15}N-enriched protein and they are extremely powerful for the analysis of the NMR spectra of larger proteins, as recently demonstrated for the 17-kDa protein interleukin-1β (*15*). However, attempts to use the same methodology for obtaining complete assignments of the protein calmodulin (16.7 kDa) were only partly successful (*16*), resulting in assignment of about 80% of the backbone ^{1}H res-

0022-2364/90 $3.00

DOI of original item: doi: 10.1016/0022-2364(90)90333-5

onances. Calmodulin presents a particularly difficult case because of the high α-helical content and the scarcity of aromatic residues in the protein core, resulting in very poor chemical-shift dispersion of both the amide and the Cα protons. Moreover, the protein consists of four homologous domains and many of the connectivity patterns found for these domains overlap with one another, making their analysis even more difficult.

We recently demonstrated that 3D triple-resonance NMR of the uniformly ^{13}C- and ^{15}N-enriched protein can be used successfully to solve the assignment problem (*17*). This required the use of four different triple-resonance experiments, in addition to the previously described ^{15}N HOHAHA-HMQC 3D pulse scheme (*14*). The present paper gives a detailed description of the novel 3D triple-resonance experiments, including a discussion of the hardware requirements needed for their implementation on commercial spectrometers.

It has long been recognized that ^{13}C–^{13}C and ^{13}C–^{15}N one-bond J couplings can be used for obtaining resonance assignments in isotopically enriched peptides and proteins (*18*). Oh, Stockman, and co-workers (*19–21*) have made extensive use of ^{13}C–^{13}C couplings to obtain resonance assignments for the proteins cytochrome *c*-553 and *Anabaena* 7120 ferredoxin and flavodoxin. The interresidue one-bond J coupling ($\sim$15 Hz) between ^{15}N and carbonyl (C′) atoms provides a source of sequential connectivity information when using ^{13}C-detected heteronuclear shift correlation experiments (*22–24*). Unfortunately, these experiments which use direct observation of the ^{13}C nucleus suffer from relatively low sensitivity and substantial resonance overlap. Moreover, because of overlap in the ^{13}C and ^{15}N spectra, assignments obtained for the low-γ nuclei often cannot be extended to the ^{1}H spectrum. The 3D experiments described in this paper overcome these problems by integrating these earlier heteronuclear 2D experiments with the 2D indirect detection experiments (*25–27*).

For making complete and unambiguous assignments of the backbone atoms of a protein we find it necessary to use at least five different 3D experiments. First, the previously described ^{15}N HOHAHA-HMQC pulse scheme correlates intraresidue NH, ^{15}N, and Hα chemical shifts. Second, a new 3D experiment referred to as HNCO correlates the NH, ^{15}N, and C′ chemical shifts. Third, a scheme named HNCA correlates NH, ^{15}N, and Cα resonances. All three 3D experiments detect the amide proton during the t_3 detection period and therefore must be performed in H_2O solution with presaturation of the H_2O resonance. The remaining two 3D experiments, HCACO and HCA(CO)N, detect the Hα proton during t_3 and they are therefore preferably recorded on samples in D_2O solution. The HCACO scheme correlates intraresidue Hα, Cα, and C′ chemical shifts. Finally, the HCA(CO)N scheme is a relay experiment correlating the Hα and Cα chemical shifts with the ^{15}N chemical shift of the succeeding residue by using the C′ nucleus as a relay intermediate. Because of the large difference in chemical shifts ($\sim$120 ppm) between the Cα and the C′ resonances these two types of nuclei can be excited separately. This has the advantage that the homonuclear C′–Cα J coupling can be easily suppressed, but it requires four different frequencies, making the experiments of the quadruple resonance type. As will be discussed later, both Cα and C′ frequencies can be generated by a single frequency synthesizer without frequency switching, simplifying the hardware requirements.

EXPERIMENTAL METHODS

Below, the magnetization transfer processes that are pertinent for the new 3D pulse schemes, shown in Figs. 1–4, are discussed in terms of the operator formalism. For simplicity, only terms that contribute to the final spectrum are retained. In this description, the effects of the pulse sequence between the end of the magnetization recovery period and the beginning of the evolution period are described by the operator **A**; the effect of the pulses and delays between the end of the t_1 period and the start of the t_2 period is represented by the operator **B**; and finally, the conversion between the end of the t_2 period and the start of the data acquisition period (t_3) is described by the operator **C**. The effects of relaxation will be neglected.

The HNCO experiment. The HNCO experiment correlates the NH and ^{15}N chemical shifts of one amino acid with the C′ shift of the preceding residue, providing crucial sequential connectivity information. This experiment essentially is the 3D analog of the ^{15}N–C′ correlation experiments (*22–24*). Figure 1 shows the pulse scheme used for this experiment. Using an INEPT sequence (*28, 29*), magnetization originating on NH protons is transferred to the directly coupled ^{15}N spin. During the t_1 period, the ^{15}N magnetization evolves exclusively under the influence of ^{15}N chemical shift as ^1H, C′, and Cα decoupling is achieved through the application of 180° pulses at the midpoint of t_1. During the following delay, δ, ^{15}N magnetization becomes antiphase with respect to the polarization of the carbonyl spin of the preceding residue ($^1J_{NC'} \approx 15$ Hz). Because the experiment is recorded in H_2O solution, and because the δ delays are relatively long (~20 ms each), it is desirable to use H_2O saturation during these periods. H_2O saturation during the t_2 period cannot easily be done with our present hardware setup. The first 90° C′ pulse converts the antiphase ^{15}N magnetization into ^{15}N–C′ two-spin (zero- and double-quantum) coherence. The contributions of ^{15}N chemical shift and ^1H–^{15}N J coupling are removed during the t_2 period by the

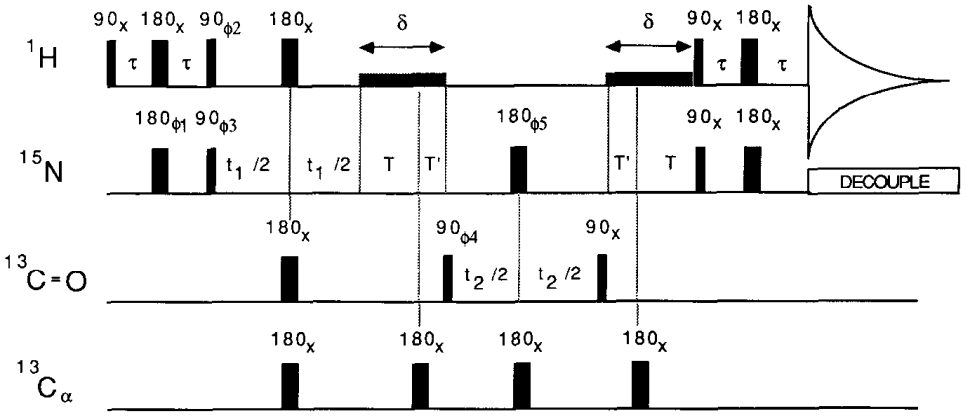

FIG. 1. Pulse scheme of the HNCO experiment. Typical delay durations used in this experiment are τ = 2.25 ms, δ = 18 ms, T = 14 ms, and T' = 4 ms. Presaturation of the H_2O resonance (not shown) is needed when the experiment is recorded in H_2O solution. In addition, water saturation is employed during both δ periods. The phase cycling used is as follows: $\phi_1 = x, -x$; $\phi_2 = y, -y$; $\phi_3 = x$; $\phi_4 = 2(x), 2(-x)$; $\phi_5 = 4(x), 4(y), 4(-x), 4(-y)$; Acq. $= x, 2(-x), x, -x, 2(x), -x$. The phases ϕ_3 and ϕ_4 are independently incremented by 90° to generate complex data in the t_1 and t_2 dimensions, respectively. In both the t_1 and t_2 dimensions, quadrature detection is achieved using the TPPI–States method (*34*).

application of the $180^{\circ}_{\phi 5}$ ^{15}N pulse. In addition, Cα–C′ decoupling is achieved by applying a 180° Cα pulse at the midpoint of t_2. At the end of the C′ evolution period, t_2, magnetization is transferred back to the NH protons by reversing the transfer steps described above. Since the NH proton is detected during t_3, the proton carrier can be placed in the center of the amide region and the spectral width in the F_3 dimension can be confined to a relatively narrow region (~8 ppm). This results in a factor of two data storage savings relative to what would be needed if the carrier were placed at the H_2O frequency. With the carrier away from the water resonance, H_2O irradiation during the relaxation delay and the two δ periods is accomplished using an off-resonance DANTE sequence (*30*).

Denoting the NH, ^{15}N, and C′ spins by I, N, and S, respectively, the HNCO pulse sequence can be described concisely by the operator formalism as

$$I_z \xrightarrow{\mathbf{A}} -2I_zN_y \xrightarrow{t_1} 2I_zN_y\cos\Omega_N t_1 \xrightarrow{\mathbf{B}} 4N_xS_yI_z\cos\Omega_N t_1 \xrightarrow{t_2}$$

$$4N_xS_yI_z\cos\Omega_N t_1\cos\Omega_S t_2\cos\pi J_{NC\alpha}t_2\{\prod_k \cos\pi J_{kS}t_2\} \xrightarrow{\mathbf{C}}$$

$$I_x\cos\Omega_N t_1\cos\Omega_S t_2\cos\pi J_{NC\alpha}t_2\{\prod_k \cos\pi J_{kS}t_2\}, \quad [1]$$

where pulse phases corresponding to the first step of the phase cycle (Fig. 1) have been assumed, and J_{kS} refers to long range coupling between the carbonyl carbon and other protons, k. For simplicity, the assumption $T' = T$ has been made and the J-coupling and chemical-shift effects which are removed by 180° pulses have been omitted in expression [1]. Ω_N and Ω_S denote the ^{15}N and C′ chemical-shift offsets and $J_{NC\alpha}$ is the intraresidue ^{15}N–Cα J coupling. The two-bond interresidue ^{15}N–Cα J coupling is often small in proteins and has been neglected in Eq. [1]. Expression [1] shows that the detected in-phase signal (I_x) is modulated in amplitude by Ω_N and Ω_S in the t_1 and the t_2 dimension, respectively, giving rise to a purely absorptive 3D NMR signal after 3D Fourier transformation. The poor digital resolution in the F_2 dimension prohibits observation of the $J_{NC\alpha}$ or $J_{HC'}$ couplings. Even if the acquisition time in the t_2 dimension were chosen much longer than is practical in a 3D experiment, the multitude of ^{15}N–Cα and small ^1H–C′ couplings would still make it difficult to resolve any individual one.

Expression [1] has been derived for the case where $T = T' = \delta/2$. However, the experiment can be conducted more efficiently with T set to a somewhat larger value than T'. For this case, the magnetization immediately before detection is described by

$$I_x\cos\Omega_N t_1\cos\Omega_S t_2\cos\{\pi J_{NC\alpha}[t_2 - 2(T - T')]\}\{\prod_k \cos\pi J_{kS}t_2\}. \quad [2]$$

By setting $T > T'$, the magnetization envelope in t_2 no longer starts at a maximum value at $t_2 = 0$, but rather reaches a maximum at $t_2 = 2(T - T')$. This process is functionally equivalent to resolution enhancement in the F_2 dimension by using a shifted sine bell weighting function. That is, for the case where $T > T'$, the envelope shape in T_2 resembles that of a sine bell shifted by $[\pi/2 - 2\pi(T - T')J_{NC\alpha}]$, instead of the regular cosine bell (90° shifted sine bell) shape. However, by carrying out the

enhancement in the manner described above, the concomitant loss in signal-to-noise ratio associated with resolution enhancement is minimized. Typically, T is set to about 10 ms longer than T', yielding a signal envelope in the t_2 dimension that is similar to that of a sine bell shifted by $\sim 50°$.

Alternatively, higher resolution in the C′ (F_2) dimension could be obtained if an INEPT-type magnetization transfer from ^{15}N to C′ were used, followed by the reverse process at the end of the t_2 period. This would make it possible to obtain complete removal of all J couplings to C′ during the t_2 evolution period. However, because the F_2 resolution is limited by digitization and not by the presence of small passive couplings, we expect that the simpler pulse scheme of Fig. 1 is more effective in practice.

The hardware setup required for the implementation of the 3D experiments will be described later. Suffice to say here that for this experiment the ^{15}N and ^{1}H pulses were generated by the standard electronics of our Bruker AM-500 spectrometer. The C′ and Cα pulses were generated using two separate synthesizers with their frequencies adjusted to coincide with the centers of the C′ and Cα regions of the ^{13}C spectrum. In order to minimize artifacts, it is important that the C′ pulses cause minimal excitation of the Cα resonances and vice versa. Commonly, this is achieved by using suitably shaped selective pulses. However, because of hardware limitations we used a different approach: rectangular pulses were employed for both C′ and Cα excitation with the RF strengths adjusted such that a 90° excitation pulse has a null in its excitation profile at the resonance frequency of the other nucleus. For proteins, the centers of the C′ and Cα resonances differ by about 120 ppm ($\sim$15 kHz on a 500 MHz spectrometer), and by adjusting both the C′ and the Cα RF field strengths to 3.9 kHz (64 μs 90° pulse width) excitation of the C′ nuclei by Cα pulses and vice versa is minimized. Finally, ^{15}N decoupling during data acquisition (t_3) was achieved using the WALTZ decoupling scheme (*31*) with a 1 kHz RF field.

The HNCA experiment. The HNCA experiment correlates ^{15}N and NH chemical shifts with the intraresidue Cα shift. The HNCA and the HOHAHA-HMQC experiments together establish intraresidue correlations between pairs of ^{15}N–NH and Cα–Hα chemical shifts, since the latter experiment links intraresidue NH, Hα, and ^{15}N shifts. The HNCA experiment uses the relatively small one-bond ^{15}N–Cα J coupling (8–12 Hz) to establish J correlations between the ^{15}N and the Cα spins. For more than half of the amino acids in calmodulin the HNCA experiment also provides sequential connectivity information by yielding (weak) correlations between NH–^{15}N pairs and the Cα shift of the preceding residue. Such correlations arise from the two-bond $^{2}J_{\mathrm{NC}\alpha}$ interresidue coupling, which can be as large as 7 Hz. Figure 2 shows the pulse scheme of the HNCA experiment. Denoting the NH, ^{15}N, and intraresidue Cα spins by I, N, and A, respectively, and the carbonyl spin of the preceding residue by C′, the evolution of magnetization during the course of the experiment can be described by

$$I_z \xrightarrow{\mathbf{A}} -2I_zN_y \xrightarrow{t_1} 2I_zN_y\cos\Omega_N t_1\cos\pi J_{\mathrm{NC}'}t_1 \xrightarrow{\mathbf{B}} -4I_yN_xA_y\cos\Omega_N t_1$$

$$\times\cos\pi J_{\mathrm{NC}'}t \xrightarrow{t_2} 4I_yN_xA_y\cos\Omega_N t_1\cos\pi J_{\mathrm{NC}'}t_1\cos\Omega_A t_2 \xrightarrow{\mathbf{C}}$$

$$I_x\cos\Omega_N t_1\cos\pi J_{\mathrm{NC}'}t_1\cos\Omega_A t_2, \quad [3]$$

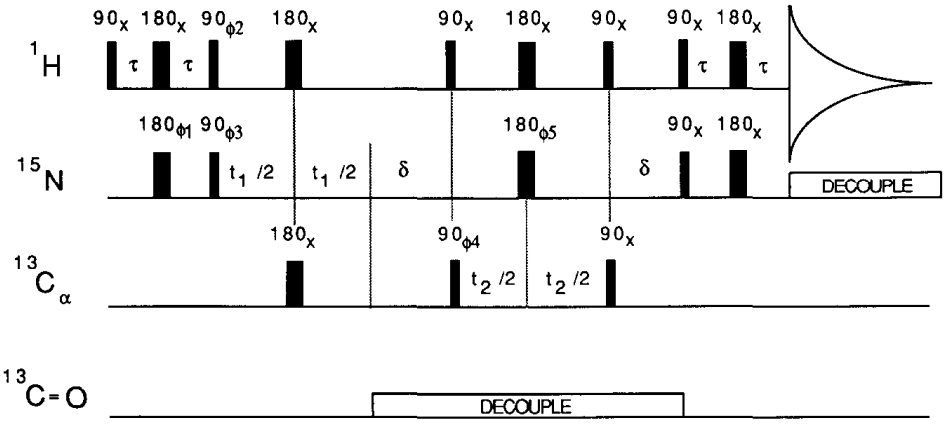

FIG. 2. Pulse sequence for the HNCA experiment. The delay δ is adjusted to be an integral multiple of $1/J_{NH}$ and to allow maximal magnetization transfer between the ^{15}N and Cα spins. Typical delay durations are δ = 33 ms and τ = 2.25 ms. The phase-cycling scheme is identical to that of the HNCO experiment (Fig. 1). ^{15}N decoupling during the t_1 period, although desirable, was technically not possible at the time the 3D spectrum was recorded.

where again terms have been neglected that originate from J coupling or chemical-shift dephasing but that later are refocused. Also, for simplicity it has been assumed that $\delta = 1/(2J_{NA})$, where J_{NA} is the one-bond N–Cα J coupling. In expression [3] Ω_N and Ω_A denote the chemical shifts of the intraresidue ^{15}N and Cα spins, and $J_{NC'}$ is the interresidue ^{15}N–C′ coupling constant. Expression [3] applies to the case where the two-bond coupling between ^{15}N and the preceding Cα spin, A′, is zero. In cases where a substantial $J_{NA'}$ two-bond coupling exists, the signal immediately prior to detection is given by

$$I_x \cos \Omega_N t_1 \cos \pi J_{NC'} t_1 \{\cos \Omega_A t_2 [\sin \pi J_{NA} \delta \cos \pi J_{NA'} \delta]^2 + \cos \Omega_{A'} t_2 [\sin \pi J_{NA'} \delta \cos \pi J_{NA} \delta]^2\} \quad [4]$$

Expressions [3] and [4] indicate that the detected signal is amplitude modulated in both the t_1 and the t_2 dimensions, leading to a pure absorption lineshape after 3D Fourier transformation. The undesirable $J_{NC'}$ coupling present during the t_1 (^{15}N) evolution period in practice does not affect the signal very much because the acquisition time in the ^{15}N dimension is typically chosen shorter than $1/(2J_{NC'})$. At the time the 3D HNCA spectrum was recorded, decoupling of the $J_{NC'}$ interaction, although desirable, was not yet possible.

The pulse scheme of Fig. 2 can be understood as follows. Magnetization originating on NH protons is transferred to their directly attached ^{15}N spins via an INEPT sequence. ^{15}N chemical-shift evolution proceeds during t_1, with Cα and ^1H decoupling achieved by the application of refocusing pulses in the middle of this period. During the subsequent delay, δ, the ^{15}N magnetization becomes antiphase with respect to the coupled Cα spin(s). This δ delay is tuned to an integral multiple of $1/J_{NH}$, so that ^{15}N magnetization remains antiphase with respect to the coupled proton. In order to minimize relaxation losses and optimize transfer for those cases where a significant two-bond

^{15}N–Cα coupling is also present, the value of δ is set to approximately $1/(3J_{NC\alpha})$, 33 ms in practice. Subsequent application of 90° pulses to both ^{1}H and Cα spins establishes three-spin NH–^{15}N–Cα coherence, as indicated in Eq. [3] by the term $I_yN_xA_y$. ^{1}H and ^{15}N chemical shifts are refocused during t_2 by the application of 180° ^{1}H and ^{15}N pulses at the midpoint of this interval, so that the total chemical-shift evolution of the three-spin coherence depends only on the Cα chemical shift. For simplicity, the effects of J-coupling evolution during t_2 caused by NH–Hα and long-range ^{15}N–^{1}H J couplings have been omitted in Eq. [3]. For proteins these couplings are typically much smaller than the "natural linewidth" of the three-spin coherence which is dominated by the short Cα T_2, and they may therefore be neglected. After the t_2 period, magnetization is transferred back to the NH protons by the reverse of the process described above. Since only NH protons are detected during t_3, the ^{1}H carrier may again be positioned in the center of the amide region to save data storage space.

At first sight, the generation of three-spin coherence for measuring Cα chemical-shift evolution may appear overly complicated. However, the number of RF pulses and phase-cycling steps needed for this solution is significantly less compared to any alternative scheme that yields ^{15}N- and ^{1}H-decoupled evolution of the Cα chemical shift. Note that the $I_yN_xA_y$ three-spin coherence evolves automatically in the absence of J couplings between any of these three spins (*32*).

As was the case for the HNCO experiment, ^{1}H and ^{15}N pulses were generated by the standard spectrometer electronics, and two separate synthesizers were used for the C′ and Cα irradiation. During the δ and t_2 periods, carbonyl decoupling was accomplished by GARP modulation (*33*) of a 500 Hz RF field. ^{15}N decoupling during data acquisition (t_3) was achieved using WALTZ modulation of a 1 kHz RF field.

The HCACO experiment. The HCACO pulse scheme, shown in Fig. 3, correlates intraresidue Hα, Cα, and C′ chemical shifts. Denoting the Hα, Cα, and C′ spins by I, A, and S, the effects of this pulse sequence can be described as

$$I_z \xrightarrow{\mathbf{A}} -2I_zA_y \xrightarrow{t_1} -4A_xI_zS_z\cos\Omega_At_1\sin\pi J_{AS}t_1\cos\pi J_{AB}t_1 \xrightarrow{\mathbf{B}}$$

$$-4S_yI_zA_z\cos\Omega_At_1\sin\pi J_{AS}t_1\cos\pi J_{AB}t_1 \xrightarrow{t_2} -4S_yI_zA_z\cos\Omega_At_1\sin\pi J_{AS}t_1$$

$$\times\cos\pi J_{AB}t_1\cos\Omega_St_2 \xrightarrow{\mathbf{C}} I_x\cos\Omega_At_1\sin\pi J_{AS}t_1\cos\pi J_{AB}t_1\cos\Omega_St_2, \quad [5]$$

where Ω_A and Ω_S are the Cα and C′ chemical shifts, J_{AS} is the Cα–C′ J coupling ($\sim$55 Hz), and J_{AB} is the Cα–Cβ J coupling ($\sim$40 Hz). For simplicity, the effect of the ^{15}N–Cα coupling during the t_1 period has been neglected. As before, the phases corresponding to the first step of the phase cycle (Fig. 3) are assumed. Expression [5] indicates that in the t_1 dimension both the active coupling, J_{AS}, and the passive coupling, J_{AB}, are present. Phasing the F_1 dimension of the spectrum to the absorption mode would result in multiplet components that are opposite in phase, distributing the intensity associated with each Hα–Cα–C′ correlation over these two antiphase F_1 doublet components. In practice, we prefer phasing the F_1 dimension to the dispersive mode. As briefly discussed below, in cases where the couplings are not fully resolved this dispersive representation can be advantageous. In the HCACO experiment, the t_1 acquisition time is set to about $1/(2J_{AB})$. In this case the $\sin\pi J_{AS}t_1\cos\pi J_{AB}t_1$ time

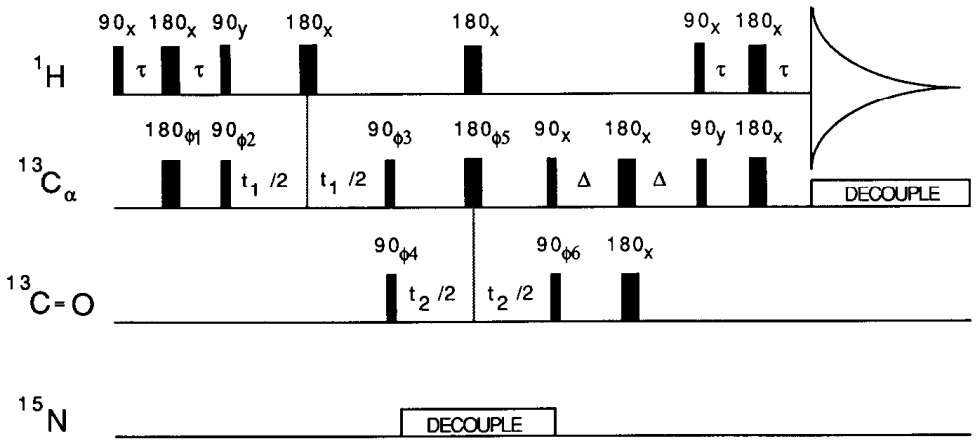

FIG. 3. Pulse sequence for the HCACO experiment. Typical delay durations are τ = 1.5 ms and Δ = 3 ms. The power levels of the Cα and C′ pulses are adjusted such that during application of a Cα pulse minimal C′ excitation occurs, and vice versa. On a 500 MHz spectrometer, for a 120 ppm difference of the C′ and Cα carrier positions, this condition may be achieved by adjusting the RF field strengths to $3.9/N$ kHz (N = 1, 2, . . .). In order to minimize the effects of homonuclear J modulation by the passive Cα–Cβ couplings during the intervals Δ, the RF field strength of the 180°_x (Cα) pulse may be reduced to 1.95 kHz. Note that because a change in power frequently also introduces a phase shift, it may be necessary to use the same low power level for the two 90°_x and 90°_y Cα pulses immediately preceding and following the Δ intervals. The phase cycling employed is as follows: $\phi_1 = x, -x$; $\phi_2 = x$; $\phi_3 = y, -y$; $\phi_4 = 2(x), 2(-x)$; $\phi_5 = 4(-x)$; $\phi_6 = 8(x), 8(-x)$; Acq. $= 2(x, -x, -x, x), 2(-x, x, x, -x)$. The phases ϕ_2 and ϕ_4 are incremented by 90° to generate complex data in the t_1 and t_2 dimensions respectively.

dependence in the t_1 dimension results in an envelope shape that is similar to that of a sine bell. Fourier transformation followed by phasing to the dispersive mode then yields a non-Lorentzian lineshape that resembles a singlet for which resolution enhancement with a sine bell filtering function is used. As Eq. [5] indicates, the lineshapes in both the F_2 and the F_3 dimension are purely absorptive.

The mechanism of the HCACO sequence is briefly outlined below. Magnetization originating on Hα is transferred to its directly attached Cα neighbor via an INEPT transfer. During the t_1 evolution period, Cα magnetization evolves under the effects of chemical shift as well as the Cα–C′ and Cα–Cβ J couplings. Hα–Cα J coupling is removed by the 180° ^{1}H pulse applied at the midpoint of t_1. Simultaneous Cα and C′ 90° pulses applied at the end of the t_1 period result in a COSY-like transfer of magnetization from Cα to C′ (and also to Cβ). Carbonyl evolution proceeds during t_2, while the net effects of ^{1}H–C′ and Cα–C′ couplings are removed by the ^{1}H and Cα 180° pulses applied at the midpoint of t_2. ^{15}N decoupling during t_2 is accomplished by ^{15}N irradiation with a WALTZ-modulated 1 kHz RF field. At the end of the t_2 period C′ magnetization is transferred back to the Cα spin. The Cα magnetization is at this point antiphase with respect to the C′ spin state. This antiphase magnetization refocuses during the following interval 2Δ. In order to minimize loss of magnetization due to relaxation and dephasing by coupling to the Cβ spin, 2Δ is set to $\sim 1/(3J_{C'C\alpha})$, 6 ms in practice. Also, to reduce dephasing due to Cα–Cβ coupling, the 180° Cα pulse applied at the midpoint of the interval 2Δ is semiselective; i.e., an RF field strength of ~2 kHz is used for this pulse, resulting in good inversion of the Cα spins, but poor

inversion of most Cβ resonances. This reduces the effects of homonuclear Cα–Cβ J modulation, increasing the overall sensitivity of the experiment. By using relatively low power for this 180° pulse, possible spurious Hα–Cα–Cβ correlations are attenuated. These spurious correlations, however, are most effectively removed by phase cycling of the phases ϕ_3, ϕ_4, ϕ_5, and ϕ_6, in a manner as indicated in the caption of Fig. 3. At the end of the interval, 2Δ, magnetization is transferred back from Cα to Hα via a reverse-INEPT sequence. Since the HCACO experiment detects Hα resonances during t_3 and does not require the presence of amide protons, it is most easily conducted in D_2O solution. The proton carrier is placed at the center of the Hα region and the spectral width in the F_3 dimension again is chosen to be quite narrow to save data storage space.

The ^{1}H, Cα, and C′ pulses are all generated by standard spectrometer electronics. The ^{13}C transmit frequency is set at the center of the Cα region, and as in the HNCO experiment, the RF power level is adjusted such that a 90° Cα pulse has a null at the center of the carbonyl region. Carbonyl 90° pulses are applied as DANTE-type pulses (*30*) using multiple repetitions of the cycle $\theta_{0°}$—$\theta_{300°}$—$\theta_{240°}$—$\theta_{180°}$—$\theta_{120°}$—$\theta_{60°}$. For the case where $\theta \ll \pi$, a single such cycle to a good approximation corresponds to a flip angle of 5.8θ, applied at an offset downfield from the carrier that equals the reciprocal of the total duration of this cycle. The difference between the centers of the Cα and C′ regions is 121 ppm which on a 500 MHz spectrometer equals 15.2 kHz. Thus, by adjusting the duration of θ to 10.96 μs, on-resonance irradiation of the C′ resonances can be accomplished without switching of the synthesizer frequency. Note that switching of the synthesizer frequency from Cα to C′ and back is undesirable because it causes problems in establishing the desired phase relationship between Cα pulses before and after the carbonyl pulse. The DANTE-type pulses have the advantage over an extra "homemade" third channel in that all phase shifting of the DANTE sequence can be accomplished with standard spectrometer software; the disadvantage is that it is difficult (although not impossible) to apply pairs of Cα and C′ pulses at exactly the same time. In our experiments, we use two repetitions of the above cycle for a 90° C′ pulse, with θ adjusted to 7.7°.

^{15}N decoupling is achieved with an additional synthesizer, using WALTZ modulation of a 1-kHz ^{15}N RF field. ^{13}C decoupling during data acquisition (t_3) is accomplished using GARP modulation (*31*) of a 4 kHz ^{13}C RF field.

The HCA(CO)N experiment. The HCA(CO)N experiment provides another source of sequential connectivity information by correlating Hα and Cα shifts of one amino acid with the ^{15}N shift of the succeeding residue. The pulse sequence of this experiment is shown in Fig. 4. Denoting the Hα, Cα, and C′ nuclei of one amino acid by I, A, and S and the ^{15}N nucleus of the succeeding residue by N, the effects of the pulse sequence can be concisely described as

$$I_z \xrightarrow{\mathbf{A}} -2I_zA_y \xrightarrow{t_1} -4A_xI_zS_z\cos\Omega_A t_1 \sin\pi J_{AS}t_1 \cos\pi J_{AB}t_1 \xrightarrow{\mathbf{B}}$$

$$-8S_xN_yI_zA_z \cos\Omega_A t_1 \sin\pi J_{AS}t_1 \cos\pi J_{AB}t_1 \xrightarrow{t_1} -8S_xN_yI_zA_z\cos\Omega_A t_1$$

$$\times \sin\pi J_{AS}t_1 \cos\pi J_{AB}t_1 \cos\Omega_N t_2 \xrightarrow{\mathbf{C}} I_x \cos\Omega_A t_1 \sin\pi J_{AS}t_1 \cos\pi J_{AB}t_1 \cos\Omega_N t_2, \quad [6]$$

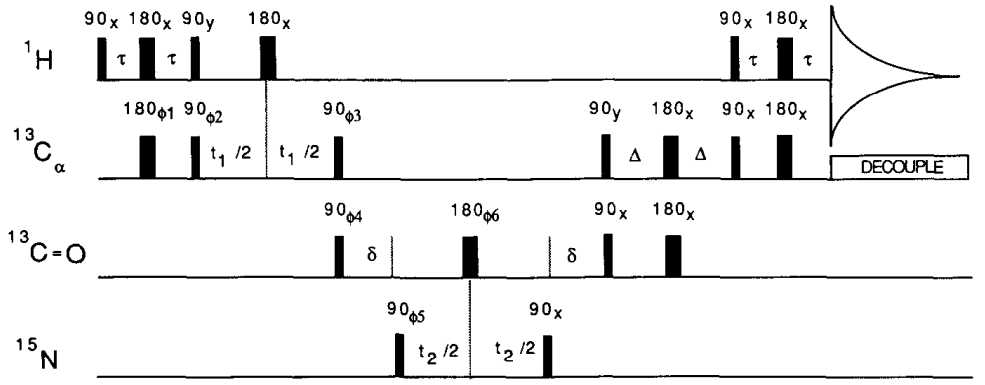

FIG. 4. Pulse scheme of the HCA(CO)N experiment. Typical delay durations are τ = 1.5 ms, Δ = 3 ms, and δ = 18–20 ms. The RF power level for the Cα and C′ pulses is adjusted in the same manner as that indicated in Fig. 3. The phase cycling employed is as follows: $\phi_1 = x, -x$; $\phi_2 = x$; $\phi_3 = y, -y$; $\phi_4 = 2(x), 2(-x)$; $\phi_5 = 4(x), 4(-x)$; $\phi_6 = 8(x), 8(y), 8(-x), 8(-y)$; Acq. $= x, 2(-x), x, -x, 2(x), 2(-x), 2(x), -x, x, 2(-x), x$. The phases ϕ_2 and ϕ_4 are incremented by 90° to generate complex data in the t_1 and t_2 dimension, respectively.

where all symbols have the same meaning as in Eq. [5], and Ω_N denotes the ^{15}N chemical shift. Again, for simplicity the presence of the small Cα–N J coupling, $J_{NC\alpha}$, has been neglected in expression [6]. Because $1/(2J_{NC\alpha})$ is smaller than either the t_1 or the t_2 acquisition period, the presence of this coupling results in a small nonresolvable broadening in the F_1 and F_2 dimensions of the spectrum.

The magnetization transfer pathway is very similar for both the HCACO and the HCA(CO)N sequences, with the exception that in the latter case magnetization transferred to the C′ spin is subsequently transferred further to the ^{15}N spin of the next residue. This is accomplished by including a period $\delta \approx 0.3/J_{NC'}$ (18 ms) during which time the C′ magnetization becomes antiphase with respect to the directly attached ^{15}N spin. The subsequent $90^\circ_{\phi 5}$ pulse generates two-spin ^{15}N–C′ coherence which evolves during t_2. The C′ $180^\circ_{\phi 6}$ pulse refocuses the effects of both C′ chemical shifts and the effects of C′–Cα J coupling so that the signal is t_2-modulated by the ^{15}N shift only. Note that C′–^{15}N correlation part of the pulse sequence is completely analogous to the regular ^1H-detected heteronuclear multiple-quantum correlation (HMQC) experiment (*26, 27*). At the end of the t_2 period, magnetization is transferred back to Hα by retracing the transfer steps discussed above. Because the presence of NH protons is not required in this type of experiment, it is most readily performed with samples in D_2O solution. Note, however, that because of a substantial isotope effect the ^{15}N shift measured for a ^{15}N–^2H site is about 0.7 ppm upfield compared to the corresponding protonated nitrogen.

Equation [6] indicates that the time-domain signal has the same t_1 envelope shape as in the HCACO experiment. As described above, we therefore prefer to phase the F_1 doublets to the antiphase dispersive mode, which gives rise to a peak shape that resembles a resolution-enhanced singlet. The lineshapes are purely absorptive in the F_2 and F_3 dimensions.

Generation of the RF for the four types of spins is accomplished in the same manner as for the HCACO experiment, discussed above.

HARDWARE REQUIREMENTS FOR TRIPLE-RESONANCE 3D SPECTROSCOPY

The 3D triple-resonance experiments discussed above put high demands on the flexibility of both spectrometer hardware and software. At present, only the most modern instruments may be able to execute these experiments without making some changes in the intrumental setup. Below, we briefly discuss the changes and additions made for our Bruker AM-500 spectrometer in order to facilitate execution of the new experiments.

First, an efficient 5-mm triple-resonance probehead of the reverse-type geometry was purchased (Bruker) which contains two coils, the inside coil tuned to ^{1}H and ^{2}H, the outside coil tuned to ^{13}C and ^{15}N.

Second, additional electronics is needed to generate the RF for the third (and fourth) channel. A scheme of the experimental setup used in the HNCA experiment is shown in Fig. 5. Most of the elements shown in this figure can be readily purchased from the instrument manufacturer or from other sources. In our case, the choice of components was determined largely by their price and by the fact that many elements already were available in our laboratory. For example, the linear class A power amplifiers used in the setup of Fig. 5 were previously used on a homebuilt solid-state NMR spectrometer.

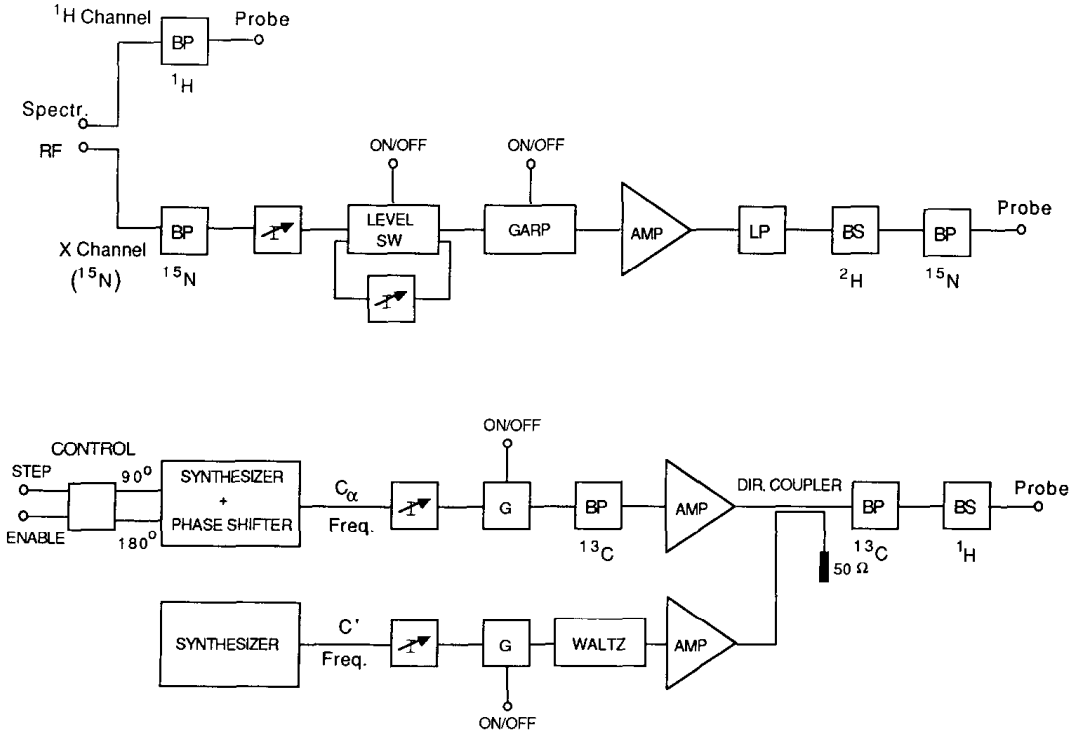

FIG. 5. Hardware configuration for the HNCA experiment. The bandpass filters (BP), RF gates (G), GARP and WALTZ modulaters, and band-stop filters (BS), as well as the directional coupler (terminated by 50 Ω) are all homebuilt. All amplifiers (AMP) are of the class A type with a maximum output power of 20 W. The RF gates each use two fast RF switches (DOTY Electronics) and in the off-mode provide more than 70 dB attenuation.

External timer. An external homebuilt timing device is not shown in Fig. 5, but significantly decreases the recording time needed for 3D spectra on Bruker AM-type spectrometers. This device takes care of automatic incrementation of either the t_1 or the t_2 evolution period of the 3D experiment, thereby greatly reducing the amount of overhead time normally needed each time t_1 or t_2 is incremented. The timing device operates by interrupting the master clock (40 MHz) that is used by the Bruker pulse sequence controller. Interfacing this device to an AM-type spectrometer requires two TTL process controller output lines and does not require any soldering. The operation of pulse sequences that do not use this external timing device is not affected by its presence. Further technical information is available upon request.

^1H channel. The spectrometer is configured to operate in the regular inverse mode, with a ^1H bandpass filter inserted between the ^1H preamplifier and the probe to prevent any of the low-γ RF power from leaking into the ^1H receiver.

X channel. The RF pulses for the nucleus that requires most extensive phase cycling (^{15}N for the HNCA experiment) are usually generated by the X channel of the spectrometer, the standard channel present on spectrometers suitable for inverse experiments. This channel has full phase-cycling capabilities and is under standard spectrometer control. Our spectrometer is not equipped with the option for fast power level switching of the X channel. Instead, we use some relatively inexpensive components to achieve this power level switching. First, the low-power output of the X channel ($\sim$1 W) is fed through a toggle switch attenuator and an appropriate bandpass filter. The subsequent power level control (Fig. 5) consists of two high-speed RF switches (DOTY Scientific) that route the RF either straight through or via a second toggle switch attenuator. Both RF switches are controlled by a single TTL level generated in the pulse program. After this switchable power level control, the RF is routed through a homebuilt module that generates the GARP modulation. Subsequently, the RF is amplified by a 20 W linear class A amplifier (ENI, Rochester, New York) and filtered through a low-pass (<250 MHz) filter, a ^2H band-stop filter, and an X-nucleus bandpass filter, before entering the probehead. The attenuator before the power level switch is manually adjusted such that, with the level switch in the high-power mode, the desired high-power RF level is obtained. This power level then can be attenuated under pulse program control by routing the RF through an additional attenuator ($\sim$6–12 dB), using the level switch.

Cα channel. The Cα frequency is derived from a synthesizer (PTS-300) that is phase-locked to the 10 MHz spectrometer master clock. The synthesizer output is routed through a toggle switch attenuator, an RF gate that is driven by a TTL level under pulse program control, into a linear 20 W class A amplifier (ENI). The amplifier output goes through the direct path of a directional coupler, via a ^{13}C bandpass and a low-pass (<250 MHz) filter to the probe. The synthesizer is equipped with a digital phase shifter. Phase cycling of the Cα channel under pulse program control can be quite cumbersome without the presence of an additional interface (*24*). In our case, we use a very simple control box to generate the desired phase cycling. This control box essentially consists of a four-step counter and its output (0, 1, 2, or 3) determines the phase of the Cα pulse (x, y, $-x$, or $-y$). The counter is advanced under pulse program control and the requested phase shift is only applied if the phase-enable TTL level is high. When both the step and enable levels are high, the counter is reset. This

simple control unit permits the execution of quite complex phase cycles in a straightforward manner.

C′ channel. The RF needed for the C′ decoupling is generated by a second synthesizer, also phase-locked to the 10 MHz master clock. Its output is attenuated, gated, and sent through a homebuilt WALTZ modulator unit. Only a very weak RF field ($\sim$500 Hz) is needed to decouple the narrow C′ region ($\sim$10 ppm) from the Cα resonances. The required power level ($\sim$0.2 W) is obtained by amplifying the WALTZ modulator output to a level of about 2 W, before sending it through the coupling port of a homebuilt directional coupler to the probe (Fig. 5).

Controlling all the hardware shown in Fig. 5 requires six TTL levels accessible under pulse program control. In addition, we use two TTL levels for the external timer, discussed above. On our spectrometer system, rearrangement of the devices discussed above provides sufficient flexibility for execution of all 3D triple-resonance experiments described in this paper.

RESULTS AND DISCUSSION

Below, the effectiveness of the 3D triple-resonance pulse schemes is demonstrated for the protein calmodulin (16.7 kDa), uniformly (>95%) enriched with ^{13}C and ^{15}N. All experiments were carried out at 47°C on a Bruker AM-500 spectrometer, modified as described above. Two samples were used: the HNCO and the HNCA experiments were carried out on a sample containing 1.5 m*M* calmodulin complexed with Ca^{2+} (6.2 m*M*) in a 93:7 H_2O:D_2O mixture, pH 6.3, 100 m*M* KCl. The HCACO and HCA(CO)N experiments were carried out on a sample containing 0.98 m*M* calmodulin (4.1 m*M* Ca^{2+}) in 99.9% D_2O, p^{2}H 6.3, 100m*M* KCl. All 3D spectra were recorded with sequential quadrature detection during the detection period (Bruker mode). In the t_1 and t_2 dimensions, complex data were acquired in a manner (*34*) that combines the advantages of the TPPI method (*35*), which yields axial peaks at the edge of the spectrum, with the favorable folding properties of the hypercomplex method of data acquisition (*36*). 3D data sets were processed in two steps. First, for processing in the t_1 dimension, routines previously developed in our laboratory (*30*) were used. Subsequently, commercially available software (NMRi, Syracuse, New York) was used to process data in the t_2 and t_3 dimensions.

Figure 6A shows the most crowded region of the NH–C′ 2D correlation spectrum, recorded with the pulse scheme of Fig. 1, but keeping the duration of the ^{15}N evolution period fixed at 2 μs. The spectrum corresponds to the projection of the 3D spectrum onto the (F_2, F_3) plane. As can be seen in the spectrum of Fig. 6A, the 2D spectrum yields a significant number of overlapping correlations. Even more important, for only a small number of NH resonances that do not overlap *in the 1D ^1H spectrum* can the ^{15}N frequency that corresponds to a particular correlation in the 2D spectrum be obtained (from a ^1H–^{15}N shift correlation spectrum). Figures 6B and 6C show slices of the 3D HNCO spectrum, taken at F_1 (^{15}N) chemical shifts of 123.6 and 119.7 ppm, respectively. The F_1 linewidth is about 0.5 ppm, so that only NH–C′ correlations are present for amides that resonate within $\pm$0.3 ppm from the ^{15}N chemical-shift value where the F_2 slice is selected. Clearly, the overlap present in the 2D spectrum is removed almost completely, and for each NH–C′ correlation the ^{15}N shift is now available.

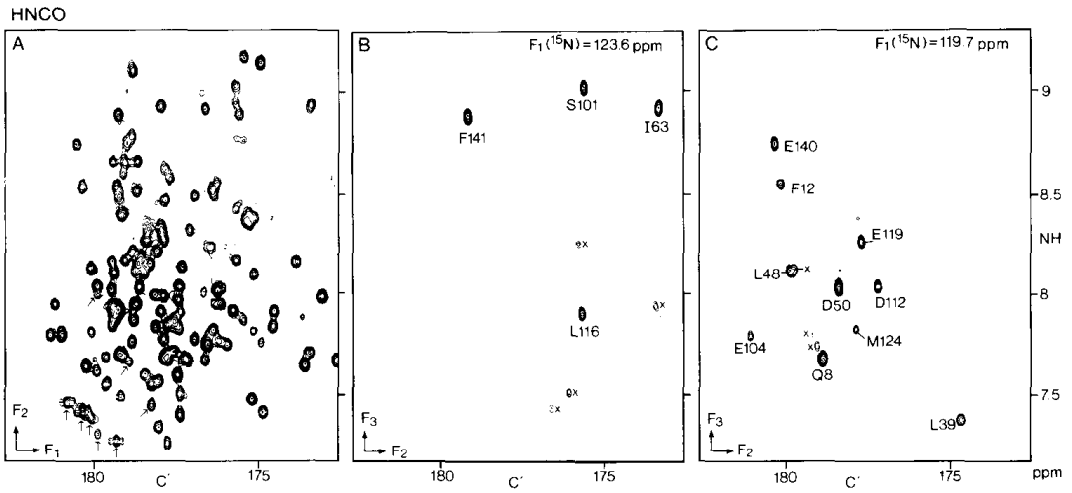

FIG. 6. (A) Section of the 2D NH–C′ correlation spectrum of calmodulin, recorded with the pulse scheme of Fig. 1 but leaving the t_1 evolution time in this pulse scheme fixed at 2 μs. Apart from higher digital resolution in the C′ dimension, this 2D spectrum corresponds to the projection onto the (F_2, F_3) plane of the 3D HNCO spectrum. Correlations for side chains of Asn and Gln residues are marked by arrows. (B, C) Sections from (F_2, F_3) slices of the HNCO 3D spectrum, taken at F_1 (^{15}N) chemical shifts of 123.6 and 119.7 ppm. The 3D spectrum results from a (32 complex) × (64 complex) × (512 real) data matrix (4 Mword), with acquisition times of 30 (t_1), 46 (t_2), and 64 (t_3) ms. After zero filling the digital resolution is 17 (F_1, ^{15}N), 5.4 (F_2, C′), and 8 Hz (F_3, NH). The 16-step phase cycle was repeated four times to obtain complex data in both the t_1 and the t_2 dimensions, resulting in 128 scans per hypercomplex (t_1, t_2) pair. Using a 1.16 s delay between scans, the total measuring time was 46 h. The delay τ was 1.5 ms, and δ was set to 18 ms. Baseline correction in the t_3 dimension of the time-domain data was used to reduce the intensity of the residual H_2O signal (*40*); no frequency-domain baseline correction or any other cosmetic procedures were used. Weak resonances due to proteolytic degradation and partial (~15%) deamidation of Gln and Asn residues are marked x. Resonances from proteolytic cleavage products are easily recognized because their intensity increases with the age of the sample.

Recording of the 2D correlation spectrum took about 4 h; recording the 3D spectrum required 43 h. Note, however, that the signal-to-noise ratio of the 3D spectrum is significantly better than for the 2D spectrum; as for most other 3D experiments, the measuring time is dictated by the minimum number of scans (16 or 32) needed per (t_1, t_2) value for phase cycling. Typically, for all triple-resonance experiments discussed here, we record a fast 2D spectrum to verify the correct hardware configuration before starting the 3D experiment.

The HNCO experiment also provides correlations for the side chains of the Asn and Gln residues. Because NH_2 resonances can be easily distinguished from NH resonances (*37, 38*), the presence of these additional connectivities does not present any problem. Side chain resonances that fall within the spectral region shown in Fig. 6A have been marked.

A (F_2, F_3) slice of the HNCA spectrum is presented in Fig. 7, showing the correlations between NH protons and Cα carbons. The intense correlations correspond to the intraresidue connectivities. Weaker correlations are observed via the two-bond interresidue ^{15}N–Cα J coupling, providing sequential connectivity information. Unfortunately, this type of intraresidue correlation is observed for only about 55% of the

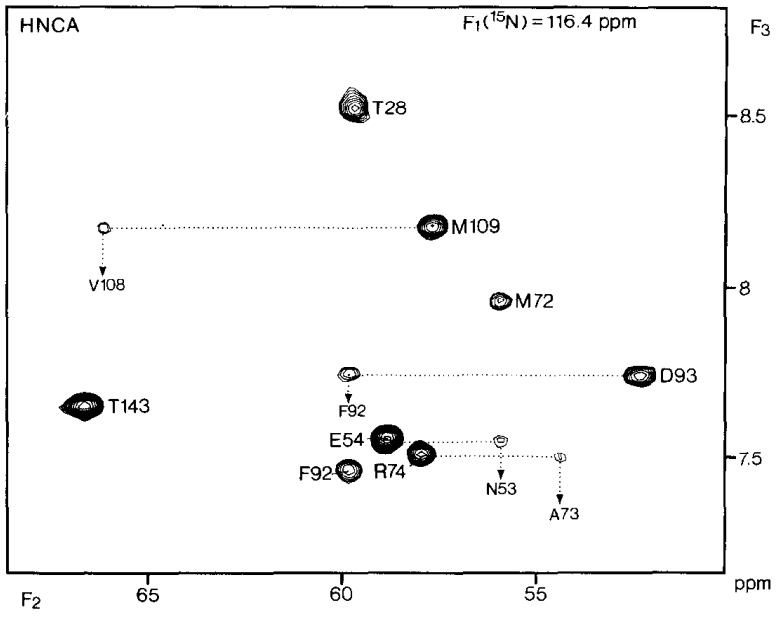

FIG. 7. Part of an (F_2 F_3) slice of the HNCA 3D spectrum, taken at an F_1 (^{15}N) chemical shift of 116.4 ppm, displaying intense intraresidue NH–Cα correlations and weaker correlations between NH and the Cα resonance of its preceding residue. The 3D spectrum results from a (32 complex) × (64 complex) × (512 real) data matrix (4 Mword), with acquisition times of 30 (t_1), 14.8 (t_2), and 64 (t_3) ms. After zero filling, the digital resolution is 17 (F_1, ^{15}N), 17 (F_2, Cα), and 8 Hz (F_3, NH). The total measuring time was 43 h. The delay τ was 1.5 ms and δ was set to 33 ms. No baseline correction was used during data processing.

residues in calmodulin; for the remainder $^2J_{N,C\alpha}$ is too small to yield observable correlations. Note that the resonance intensity of correlations via these small couplings shows a nearly quadratic dependence on $^2J_{N,C\alpha}$ (Eq. [4]). A preliminary analysis of the HNCA 3D spectra recorded for calmodulin and for the protein interleukin-1β (*39*) does not show any obvious correlation between the intensity of the two-bond correlation and the protein backbone conformation.

In the HNCA spectrum, we also observe a number of H–N–Cγ and H–N–Cβ connectivities for the side chains of Gln and Asn residues. These correlations result from the two-bond $J_{N,C\gamma}$ and $J_{N,C\beta}$ couplings and are relatively weak.

Figure 8 shows a typical slice taken from the HCACO spectrum, displaying intraresidue correlations between Hα resonances and carbonyl carbons for residues with a Cα shift of 55.8 ± 0.5 ppm. Because the resonance dispersion of both Hα and Cα is relatively poor (compared to their linewidth), and because the lineshape in the F_1 dimension is not absorptive, some overlap of resonances is also present in this type of 3D spectrum. For example, in the slice shown in Fig. 8, the correlations for Gln-3 and Lys-115 overlap to an extent where it is not easy to identify accurately their (F_1, F_2, F_3) coordinates in an automated manner. The C′ chemical shifts measured from the HCACO spectrum are matched with the C′ chemical shifts measured with the HNCO experiment (after correcting for a small ~0.08 ppm ^{2}H isotope effect), thus providing sequential connectivity information.

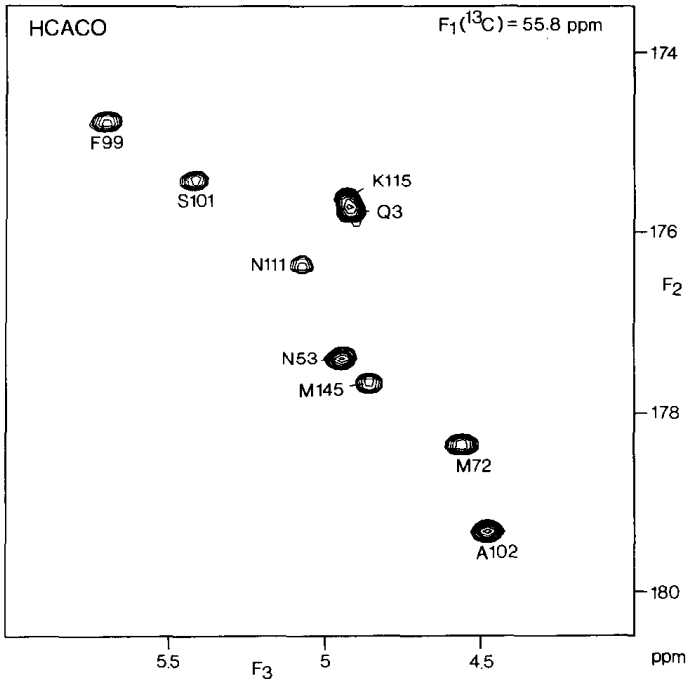

FIG. 8. Part of an (F_2, F_3) slice of the HCACO 3D spectrum, taken at an F_1 (Cα) chemical shift of 55.8 ppm, displaying intraresidue Hα–C′ correlations. The 3D spectrum results from a (32 complex) × (64 complex) × (512 real) data matrix (4 Mword), with acquisition times of 11.5 (t_1), 46 (t_2), and 64 (t_3) ms. After zero filling, the digital resolution is 43 (F_1, Cα), 11 (F_2, C′), and 8 Hz (F_3, Hα). Because of the relatively short Hα longitudinal relaxation time (~0.7 s) a short 0.75 s relaxation delay was used, resulting in a total measuring time of 32 h. The delay τ was 1.5 ms, and Δ was set to 3 ms. No baseline correction was used during data processing.

In addition to the correlations to the backbone carbonyl resonances, the HCACO spectrum also yields correlations between the side chain carbonyl resonance of Asp, Asn, Glu, and Gln residues, and the adjacent methylene resonances. Because the methylene carbons resonate between 32 and 39 ppm, well upfield from the Cα region, they are only weakly excited by the semiselective 180° Cα pulse, applied at the midpoint of the interval 2Δ in the pulse scheme of Fig. 3. Thus, the correlations observed for side chain carbonyls in the HCACO experiment are much weaker than the correlations to the backbone carbonyl resonances. Moreover, because the methylene protons usually resonate well upfield from the Hα protons, the presence of these additional correlations does not pose any problems.

Finally, Fig. 9 shows a slice taken from the HCA(CO)N relay spectrum, displaying connectivity between the Hα resonances of residues with a Cα shift of 55.8 ± 0.5 ppm and the ^{15}N shift of the succeeding residue. This slice corresponds to the same Cα shift as the slice of Fig. 8. Therefore, correlations for the same residues are observed, with the exception of Met-145 for which the correlation falls outside the spectral window shown (^{15}N of Thr-146 resonates at 110.0 ppm). Matching the ^{15}N shifts observed in the HCA(CO)N spectrum with the ^{15}N shifts measured in the HNCA and HNCO) spectra provides another source of sequential connectivity. Note that the

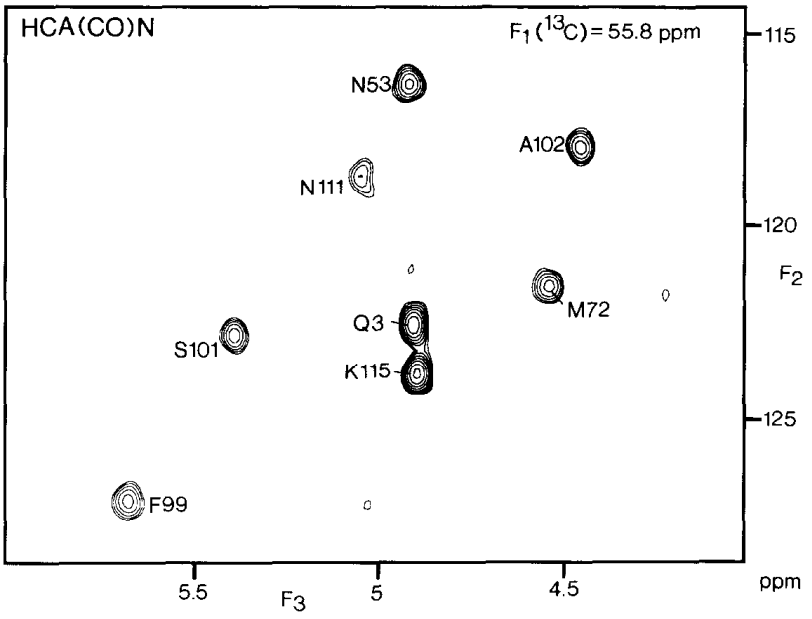

FIG. 9. Part of an (F_2, F_3) slice of the HCA(CO)N 3D spectrum, taken at an F_1 (Cα) chemical shift of 55.8 ppm, displaying interresidue Hα–^{15}N correlations. The 3D spectrum results from a (32 complex) × (32 complex) × (512 real) data matrix (2 Mword), with acquisition times of 11.5 (t_1), 30 (t_2), and 64 (t_3) ms. After zero filling, the digital resolution is 43 (F_1, Cα), 17 (F_2, ^{15}N), and 8 Hz (F_3, Hα). A 0.75 s relaxation delay was used, resulting in a total measuring time of 32 h. The delay τ was 1.5 ms, Δ was set to 18 ms, and Δ was set to 3 ms. No baseline correction was used during data processing.

^{15}N shifts measured in D_2O and H_2O samples differ substantially (~0.7 ppm) because of the ^{2}H isotope effect.

As demonstrated elsewhere (*17*), the four new experiments together with the previously described ^{15}N HOHAHA-HMQC 3D experiment provide sufficient information to obtain complete ^{1}H, ^{13}C, and ^{15}N assignments, without relying on NOE information. Therefore, these methods make it possible to obtain complete sequential assignments in a manner that is largely independent of the protein backbone conformation.

The methods described above clearly can generate high-quality 3D spectra for low concentrations (~1 mM) of relatively large proteins. The sensitivity of the methods is high because all magnetization transfer steps occur via J couplings that, with the exception of $^2J_{N,C\alpha}$, are well resolved for proteins with correlation times shorter than ~10 ns. When the correlation time is increased to about 15 ns, corresponding to a ~25 kDa globular monomeric protein at 30°C, the ^{15}N linewidth becomes comparable to the $^1J_{N,C\alpha}$ coupling, rapidly decreasing the sensitivity of the HNCA experiment. At a correlation time of ~20 ns, the ^{15}N linewidth becomes comparable with the $^1J_{N,C'}$ coupling, reducing the sensitivity of the HNCO experiment. Of the two remaining experiments, the HCA(CO)N relay experiment has lower intrinsic sensitivity compared to HCACO, because of the two relay steps involved in the transfer of magnetization from C′ to ^{15}N and back. The sensitivity of both experiments is expected to decrease rapidly for correlation times larger than ~20 ns. Note that for high sensitivity the Cα linewidth must be narrow compared to $^1J_{C\alpha,C'}$ (~55 Hz), and the C′ linewidth must

be small relative to $^1J_{C',N}$ ($\sim$15 Hz). As pointed out before, in addition to the new triple-resonance experiments, the ^{15}N HOHAHA-HMQC experiment is needed for determining the intraresidue connectivity patterns. The effectiveness of this experiment depends on the NH–Hα J coupling and on the NH and Hα linewidths. For calmodulin, all nonexchanging amide protons showed an observable correlation despite the fact that nearly half the NH–Hα couplings are 5 Hz or smaller. However, for correlation times larger than $\sim$10 ns it is expected that many of the NH–Hα correlations arising from J couplings smaller than 5 Hz will become vanishingly weak. It therefore may be expected that the assignment approach based on the methods described above will be applicable for proteins up to about 20 kDa. For larger proteins, the sensitivity of some of the 3D experiments will decrease rapidly, requiring longer measuring times, higher sample concentrations, or additional methods such as 3D NOESY or selective labeling to complete the assignment process.

Although recording of five 3D spectra at first sight may appear laborious, it should be noted that all spectra can be recorded in a total of less than 10 days. The data matrix sizes can all be relatively small, 2–8 Mword, depending on the type of experiment. Data processing and storage therefore do not impose any unusual problems. Because of the low level of resonance overlap in the 3D spectra, much of the 3D peak picking can be done in a fully automated manner. Automated analysis of the resulting resonance coordinate tables obtained for each 3D spectrum is then quite straightforward (*17*), thus dramatically reducing the amount of human intelligence (!) and labor required in the assignment process.

ACKNOWLEDGMENTS

We thank Dr. Claude Klee for stimulating discussions and continuous encouragement, Marie Krinks for assistance in preparing the sample of calmodulin used in this study, and Dr. Kathy Beckingham for providing us with the *Drosophila* calmodulin coding construct. We also thank Drs. Dennis Torchia, Marius Clore, Paul Driscoll, and Angela Gronenborn for useful suggestions during the development of the new methods described in this paper. This work was supported by the Intramural AIDS Antiviral Program of the Office of the Director of the National Institutes of Health. L.E.K. acknowledges financial support from the Medical Research Council of Canada and the Alberta Heritage Trust Foundation.

Note added in proof. Recent experiments indicate that the sensitivity of both the intra- and especially the interresidue HNCA correlations can be improved by setting the delay δ to 22 ms instead of 33 ms. Under these conditions, nearly all interresidue HNCA correlations were observed.

REFERENCES

1. K. WÜTHRICH, "NMR of Proteins and Nucleic Acids," Wiley, New York, 1986.
2. G. M. CLORE AND A. M. GRONENBORN, *CRC Crit. Rev. Biochem. Biol.* **24,** 479 (1989).
3. L. P. MCINTOSH, R. H. GRIFFEY, D. C. MUCHMORE, C. P. NIELSON, A. G. REDFIELD, AND F. W. DAHLQUIST, *Proc. Natl. Acad. Sci. USA* **84,** 1244 (1987).
4. L. P. MCINTOSH, F. W. DAHLQUIST, AND A. G. REDFIELD, *J. Biomol. Struct. Dyn.* **5,** 21 (1987).
5. H. SENN, G. OTTING, AND K. WÜTHRICH, *J. Am. Chem. Soc.* **109,** 1090 (1987).
6. D. A. TORCHIA, S. W. SPARKS, AND A. BAX, *Biochemistry* **27,** 5135 (1988).
7. D. A. TORCHIA, S. W. SPARKS, AND A. BAX, *Biochemistry* **28,** 5509 (1989).
8. D. L. LEMASTER AND F. M. RICHARDS, *Biochemistry* **27,** 142 (1988).
9. S. W. FESIK, J. R. LULY, J. W. ERICKSON, AND C. ABAD-ZAPATERO, *Biochemistry* **27,** 8297 (1988).
10. R. H. GRIFFEY AND A. G. REDFIELD, *Rev. Biophys.* **19,** 51 (1987).

11. S. W. FESIK AND E. R. P. ZUIDERWEG, *J. Magn. Reson.* **78,** 588 (1988).
12. D. MARION, L. E. KAY, S. W. SPARKS, D. A. TORCHIA, AND A. BAX, *J. Am. Chem. Soc.* **111,** 1515 (1989).
13. E. R. P. ZUIDERWEG AND S. W. FESIK, *Biochemistry* **28,** 2387 (1989).
14. D. MARION, P. C. DRISCOLL, L. E. KAY, P. T. WINGFIELD, A. BAX, A. M. GRONENBORN, AND G. M. CLORE, *Biochemistry* **28,** 6150 (1989).
15. P. C. DRISCOLL, G. M. CLORE, D. MARION, P. T. WINGFIELD, AND A. M. GRONENBORN, *Biochemistry,* **29,** 3542 (1990).
16. M. IKURA, D. MARION, L. E. KAY, H. SHIH, M. KRINKS, C. B. KLEE, AND A. BAX, *Biochem. Pharmacol.,* in press.
17. M. IKURA, L. E. KAY, AND A. BAX, *Biochemistry,* **29,** 4659 (1990).
18. M. LLINAS, D. M. WILSON, AND M. P. KLEIN, *J. Am. Chem. Soc.* **99,** 6846 (1977).
19. B. H. OH, W. M. WESTLER, P. DARBA, AND J. L. MARKELY, *Science (Washington D.C.)* **240,** 908 (1988).
20. B. J. STOCKMAN, W. M. WESTLER, P. DARBA, AND J. L. MARKLEY, *J. Am. Chem. Soc.* **110,** 4095 (1988).
21. B. J. STOCKMAN, M. D. REILY, W. M. WESTLER, E. L. ULRICH, AND J. L. MARKLEY, *Biochemistry* **28,** 230 (1989).
22. W. M. WESTLER, B. J. STOCKMAN, AND J. L. MARKLEY, *J. Am Chem Soc.* **110,** 6256 (1988).
23. W. P. NIEMCZURA, G. L. HELMS, A. S. CHESNICK, R. E. MOORE, AND V. BORNEMANN, *J. Magn. Reson.* **81,** 635 (1989).
24. E. S. MOOBERRY, B. H. OH, AND J. L. MARKLEY, *J. Magn. Reson.* **85,** 147 (1989).
25. G. BODENHAUSEN AND D. J. RUBEN, *Chem. Phys. Lett.* **69,** 185 (1980).
26. M. R. BENDALL, D. T. PEGG, AND D. M. DODDRELL, *J. Magn. Reson.* **52,** 81 (1983).
*27.*A. BAX, R. H. GRIFFEY, AND B. L. HAWKINS, *J. Magn. Reson.* **55,** 301 (1983).
28. G. A. MORRIS AND R. FREEMAN, *J. Am. Chem. Soc.* **101,** 760 (1979).
29. D. P. BURUM AND R. R. ERNST, *J. Magn. Reson.* **39,** 163 (1980).
30. L. E. KAY, D. MARION, AND A. BAX, *J. Magn. Reson.* **84,** 74 (1989).
31. A. J. SHAKA, J. KEELER, AND R. FREEMAN, *J. Magn. Reson.* **53,** 313 (1983).
32. R. R. ERNST, G. BODENHAUSEN, AND A. WOKAUN, "Principles of Nuclear Magnetic Resonance in One and Two Dimensions," p. 29, Eq. 2.1.97, Clarendon Press, Oxford, 1987.
33. A. J. SHAKA, P. BARKER, AND R. FREEMAN, *J. Magn. Reson.* **64,** 547 (1985).
34. D. MARION, M. IKURA, R. TSCHUDIN, AND A. BAX, *J. Magn. Reson.* **85,** 393 (1989).
35. D. MARION AND K. WÜTHRICH, *Biochem. Biophys. Res. Commun.* **113,** 967 (1983).
36. D. J. STATES, R. A. HABERKORN, AND D. J. RUBEN, *J. Magn. Reson.* **48,** 286 (1982).
37. L. E. KAY AND A. BAX, *J. Magn. Reson.* **84,** 598 (1989).
38. A. BAX, M. IKURA, L. E. KAY, D. A. TORCHIA, AND R. TSCHUDIN, *J. Magn. Reson.,* **86,** 304 (1990).
39. P. C. DRISCOLL, A. BAX, L. E. KAY, G. M. CLORE, AND A. M. GRONENBORN, unpublished results.
40. D. MARION, M. IKURA, AND A. BAX, *J. Magn. Reson.* **84,** 425 (1989).